Clinical Magnetic Resonance Imaging with Nuclear Medicine Correlation

Madan V. Kulkarni, Martin P. Sandler, Max I. Shaff, Jerome P. Jones, James A. Patton, C. Leon Partain, and A. Everette James

Imaging Division, Department of Radiology and Radiological Sciences, Vanderbilt University Medical Center, Nashville, Tennessee

The current role of magnetic resonance imaging (MRI) in different organ systems is discussed and compared to nuclear medicine and to other available clinical diagnostic modalities. The value of optimizing radiofrequency pulse sequence selection to provide additional tissue characterization is also described. The results of nuclear medicine and MRI studies in 56 patients are compared to evaluate the clinical diagnostic contribution of each imaging modality for various pathological processes. In addition, the state-of-the-art MRI systems and future development in MRI technology with its potential contribution is defined.

J Nucl Med 26:944–957, 1985

Although magnetic resonance imaging is in the early stages of its development, the ability to provide anatomical information comparable to both x-ray computed tomography and ultrasound, as well as to provide functional imaging information comparable to nuclear medicine examinations, has been demonstrated (*1*). Spatial resolution of x-ray computed tomography (CT) at present is slightly superior to magnetic resonance imaging (MRI), but direct coronal and sagittal images provided by MRI contribute significant new anatomical diagnostic information (*2*). Using various radiofrequency pulse sequences with MRI enhances soft-tissue contrast differences. This results in increased sensitivity of MRI to identify pathological lesions as compared to conventional radiographic procedures. The use of in vivo spectroscopy in tissue characterization has further increased the potential value of MRI in functional imaging.

Proton density, proton motion (as in flowing blood), and relaxation parameters (referred to as longitudinal [T_1] and transverse [T_2] relaxation times) contribute to the signal acquired in MRI from a given point within the patient. Damadian (*3*) has shown that some tumors have increased T_1 and T_2 proton relaxation times, as compared to the surrounding normal tissue of the same organs. By changing pulse sequences, the information regarding T_1 and T_2 relaxation parameters in abnormal tissue can be compared to the normal tissue. At this stage of MRI technology, clinical studies utilize the hydrogen atom (proton) for imaging.

Certain disadvantages are associated with MRI. In the first instance, ferromagnetic material contained in certain life-sustaining apparatus such as surgical clips (*4*), prostheses, and pacemakers (*5*) may be absolute contraindications to the performance of MR examinations. In addition, the long scanning times required may result in suboptimal images due to motion artifact. Prolonged imaging times, at present, limit MRI's ability to perform high temporal resolution dynamic imaging as compared to nuclear medicine. The magnetic field produced by the MR scanner may interfere with nearby electronic apparatus. Similarly, the presence of material containing ferrous or ferromagnetic particles might affect the magnetic field, and influence the site selection, and installation of MR scanners (*6*). Unlike nuclear medicine, MRI cannot be performed as a portable study.

The basic principles of magnetic resonance have been described (*7–9*). Two basic pulse sequences that are utilized for these images are termed spin-echo (SE) and inversion spin echo (ISE) (Fig. 1). The relative T_1 contrast between the tissue can be examined with ISE sequences (Fig. 1B) and SE sequences that have short TE and TR values (Fig. 1A). By prolonging TE as well as TR intervals, relative T_2 weighted images can be obtained.

Magnetic resonance imaging has proven to be a valuable modality in studying intracranial, cervical, thoracic, abdominal, and skeletal diseases (*9–27*). In addition

Received Dec. 17, 1984; revision accepted May 15, 1985.

For reprints contact: Madan V. Kulkarni, MD, Dept. of Radiology and Radiological Sciences, Vanderbilt University Medical Ctr., Nashville, TN 37232.

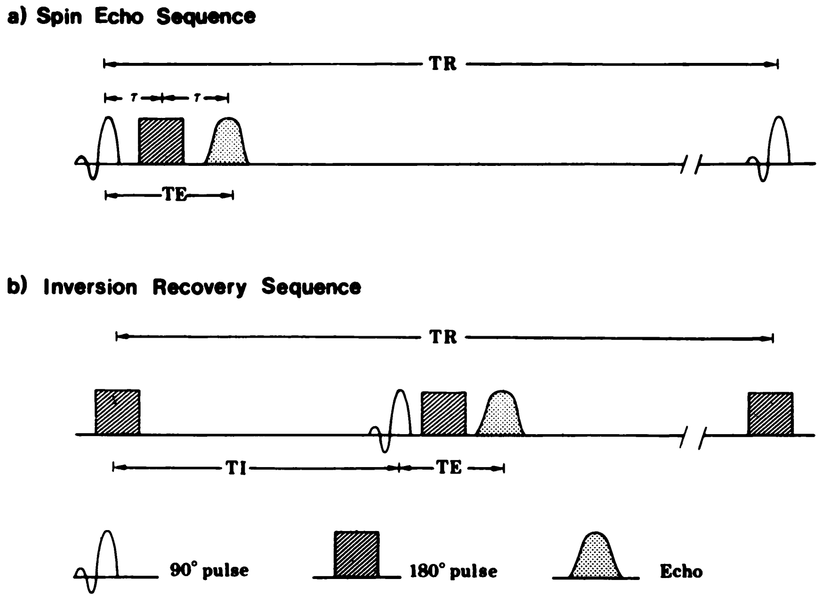

FIGURE 1
Pulse sequence diagram showing (a) spin-echo and (b) inversion recovery (T_1 weighted) sequences. By increasing TE interval, there is relative increase in T_2 information in image

to providing good spatial resolution, MRI has demonstrated excellent soft-tissue contrast and early detection of pathological abnormalities. Nuclear medicine studies also provide early detection of pathological lesions, although the spatial resolution is inferior to MRI imaging. Our initial experience with a 0.5 tesla superconducting magnet indicates excellent MRI imaging potential, enhanced by the ability of varying pulse sequences to provide T_1 and T_2 weighted images which improve tissue contrast and image detectability.

Central nervous system

Magnetic resonance has evolved as a primary imaging modality in depicting many intracranial and spinal cord abnormalities. The availability of direct coronal and sagittal imaging has improved the understanding of intracranial anatomy, and the localization of intracranial pathology (*11*). The brainstem and middle cranial fossa are particularly well imaged by MR. Computed tomography examination of these areas is somewhat limited due to streak artifacts caused by beam hardening in the temporal lobes and in the region of the brainstem. The diagnosis of syringomyelia in the cervical cord can be made on a sagittal MRI performed through the cervical cord in that it shows an area of decreased signal intensity in the middle of the cervical spinal cord and has the same signal intensity as cerebrospinal fluid (CSF) surrounding the spinal cord (Fig. 2A).

Fluids such as CSF have prolonged T_2 relaxation times. The tissues with prolonged T_2 relaxation times have increased signal intensity on T_2 weighted images as compared to the tissues with shorter T_2 relaxation times. In Fig. 2B the pulse sequences with TE of 120 and TR of 2,000 provide T_2 weighted images which demonstrate intense signals from CSF surrounding the spinal cord and within the syrinx cavity. The tissues which have prolonged T_1 relaxation times, unlike tissues with prolonged T_2 relaxation times, show decreased signal intensity on the images with pulse sequences which are T_1 weighted (i.e., SE 30/500 & ISE). Tissues with prolonged T_1 relaxation times are depicted as darker structures on SE 30/500 pulse sequences when compared to tissues with shorter T_1 relaxation times.

Direct sagittal and coronal MR images performed in the region of the brainstem and spine are superior when compared to the reconstructed sagittal and coronal images of the spine performed by CT. The tissue contrast is superior and intrathecal contrast with an agent such as metrizamide is not necessary to diagnose syringomyelia or spinal cord enlargement. The brainstem and middle cranial fossa are particularly well imaged by MRI.

Magnetic resonance imaging has demonstrated high sensitivity in the diagnosis of demyelinating diseases such as multiple sclerosis (*12*). In the evaluation of the intracranial neoplasm we have noted higher sensitivity of MRI as compared to CT. Unlike radionuclide brain scans where the isotope localization in the intracranial lesions depends on interruption of the blood-brain barrier, MRI identifies abnormalities because of increase in mobile hydrogen atoms.

Araki et al. suggested that the malignant neoplasms have longer T_1 relaxation times when compared to benign tumors (*14*). In our experience, it is not possible to distinguish tumor from edema, because both entities produce abnormal signals on T_1 and T_2 weighted images. In a patient with progressive multifocal leukoencephalopathy, the MR image shows an area of increased signal intensity in the right frontal region (Fig. 3A). Figure 3B demonstrates the use of different pulse

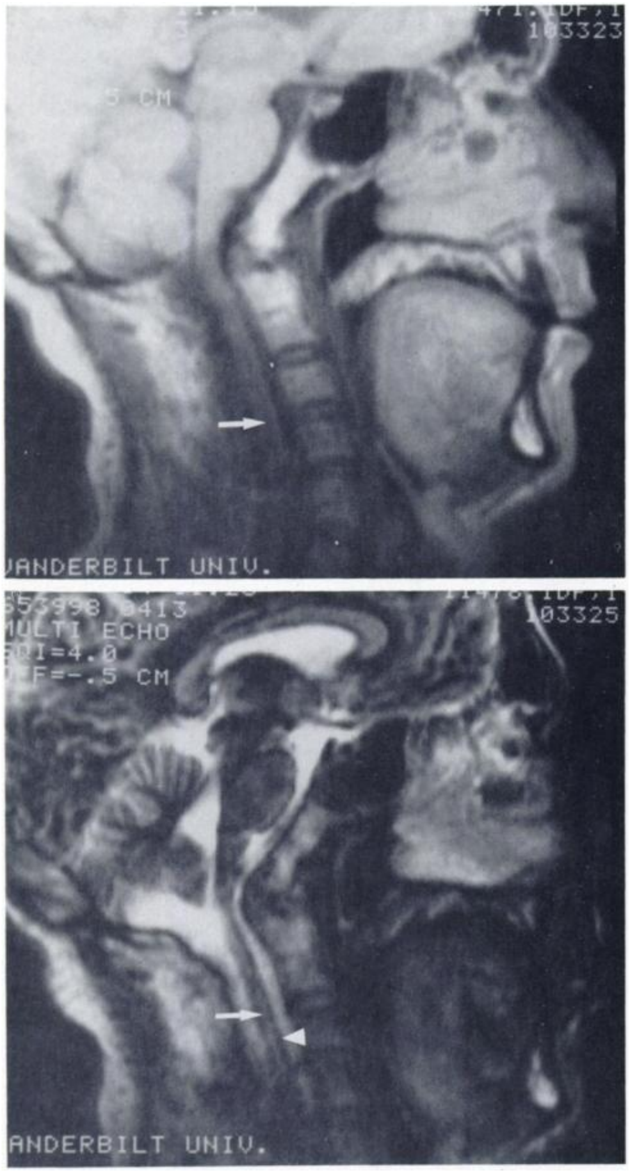

FIGURE 2
Top: Sagittal MRI image with SE 30/500 (TE = 30 msec, TR = 500 msec) pulse sequence demonstrates decreased signal intensity within the syringomyelia (arrow) in spinal cord. Bottom: On T_2 weighted pulse sequence (SE 120/2,000) syrinx has intense signal (arrow) similar to signal from CSF surrounding the spinal cord. Cervical cord (arrowhead) is seen as area of decreased signal intensity within CSF which has prolonged T_2 relaxation time

sequences in detecting the lesion. With spin-echo (SE 30/1,000) images with short TE (30 msec) and TR (1,000 msec), the mass effect on the right lateral ventricles and the midline shift are well depicted. With increased TE (Fig. 3B), increasing signal intensity is noted in the right frontal region. Using a SE 120/1,000 image (Fig. 3B, bottom left) the abnormality is seen as an intense signal, although the lateral ventricles are not well depicted using this pulse sequence. These T_2 weighted images (prolonged TE) have been found most sensitive in detecting abnormalities. Radionuclide brain scan (Fig. 3C) can also demonstrate the abnormality but the mass effect and midline shift are better documented with MRI. Inflammatory lesions may be detected on MR images, and preliminary work in the use of paramagnetic contrast agents in animal brain abscess models at Vanderbilt has indicated that paramagnetic contrast enhancement with MRI is superior to nuclear medicine (*29*). The use of intravenous paramagnetic contrast agents may help to make the differentiation between neoplastic and inflammatory lesions.

Neck

The evaluation of the thyroid and other neck masses by MR provides valuable information. Nuclear medicine examination of a thyroid nodule provides information regarding the uptake and organification of iodine. Fluorescent scanning quantitates the iodine content within the abnormal thyroid nodule to predict the probability of benignancy within the nodule (*30*).

A technetium-99m (^{99m}Tc) pertechnetate thyroid scan in a patient with thyroid adenoma demonstrated decreased radioactivity in the left lobe of the thyroid gland (Fig. 4A). The MR image showed an area of abnormality in the left lobe of the thyroid gland on a SE 30/500 sequence (Fig. 4B). When a T_2 weighted image was performed (SE 60/1,000) in the same region, the abnormality demonstrated increased signal intensity, suggesting a longer T_2 value within the adenoma when compared to the rest of the thyroid gland. Magnetic resonance imaging has shown prolonged T_1 and T_2 relaxation times in solid thyroid nodules (*17*). In a small series of patients with mediastinal thyroid radioisotope studies, it was not possible to detect mediastinal extension of the goiter in three out of seven patients (*16*). Magnetic resonance imaging can detect these masses and separate them from the major vessel in the mediastinum. In this respect, MRI appears to be superior when compared to CT, since the use of i.v. contrast is not needed to separate soft tissue densities from the blood vessels, and sagittal and coronal imaging can be performed to demonstrate mediastinal extensions more effectively (*18*). Hemorrhage in thyroid nodules can be diagnosed because of short T_1 values of a resolving hematoma. Functioning mediastinal thyroid tissue has also been shown to have relatively increased T_1 and T_2 values (*17*).

In a recent communication, Stark et al. have suggested that both the neck and the thoracic inlet can be examined by MRI without streak artifact and that vascular structures can be separated from soft tissue masses without the infusion of i.v. contrast material (*15*). We have also detected abnormal lymph node enlargement in the neck with MRI because its signal intensity is different from both the muscle and the

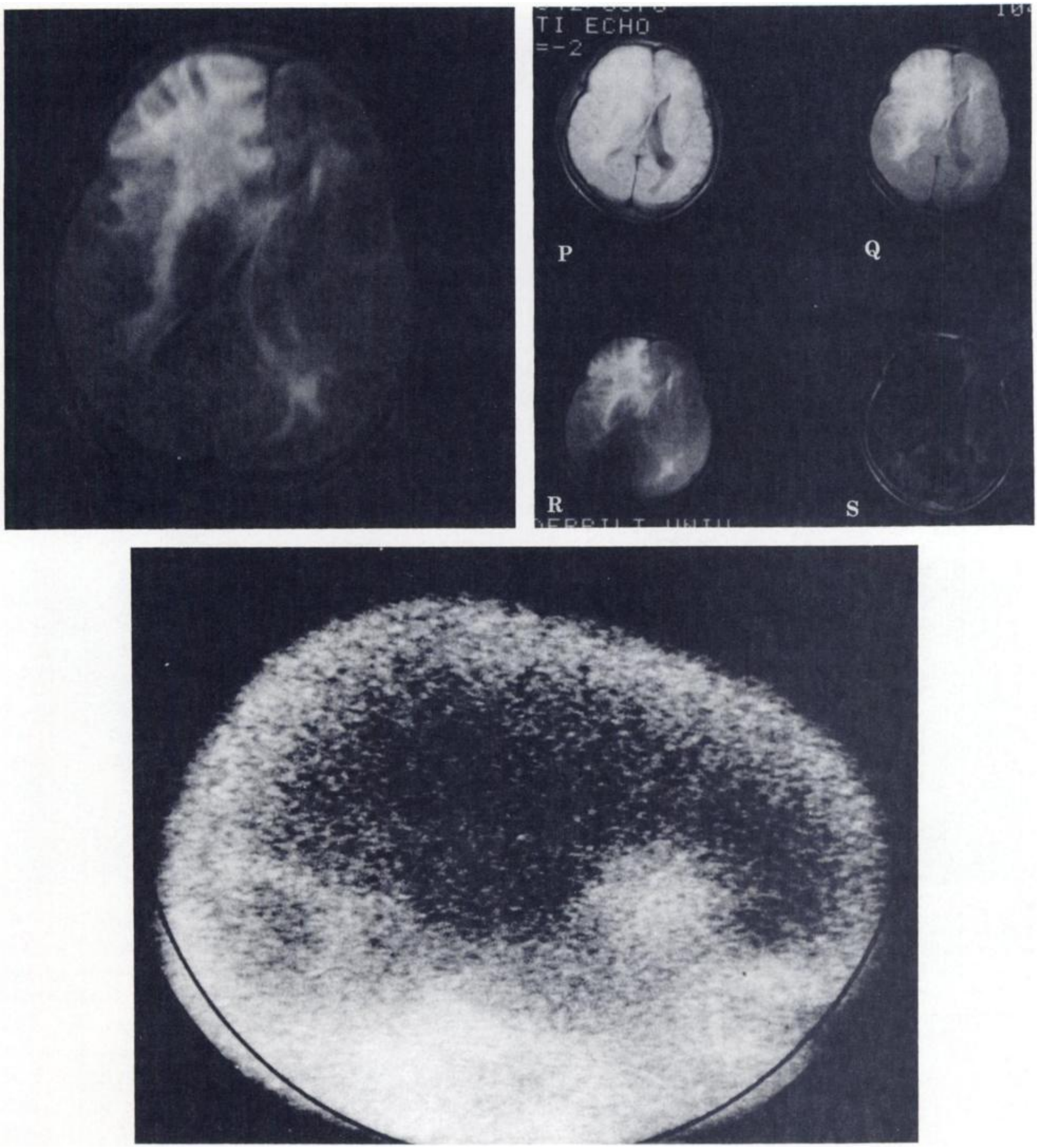

FIGURE 3
Top (left): Magnetic resonance image in transverse plane using SE 120/1,000 sequence (T_2 weighted) demonstrates marked increase in signal intensity in right frontal lobe. There is slightly decreased signal intensity within center of lesion. Apparent area of abnormality is larger on MR scan. Top (right): Use of different pulse sequences at same transverse level demonstrates that contrast between frontal lobe abnormality and normal brain is seen in SE 120/1,000 (R) and IR 30/450/1500 (S) images which are T_2 and T_1 weighted images, respectively. Although SE 30/1,000 (P) image does not show good contrast between abnormality and normal brain, mass effect on the right lateral ventricle is better using this pulse sequence. At biopsy, this abnormality was determined to be focus of progressive multifocal leukoencephalopathy. Bottom: [^{99m}Tc]glucoheptonate brain scan demonstrates increased activity in frontal lobe on right lateral view. Abnormality is clearly demonstrated, but mass effect and midline shift are seen only on MRI

vascular structures in this area. The contrast provided by MRI between the muscle and lymphadenopathy is superior to the contrast between lymph node enlargement and muscle provided by a similar CT scan. Since there is no appreciable signal in normal blood vessels, MRI does not require the use of contrast agents to

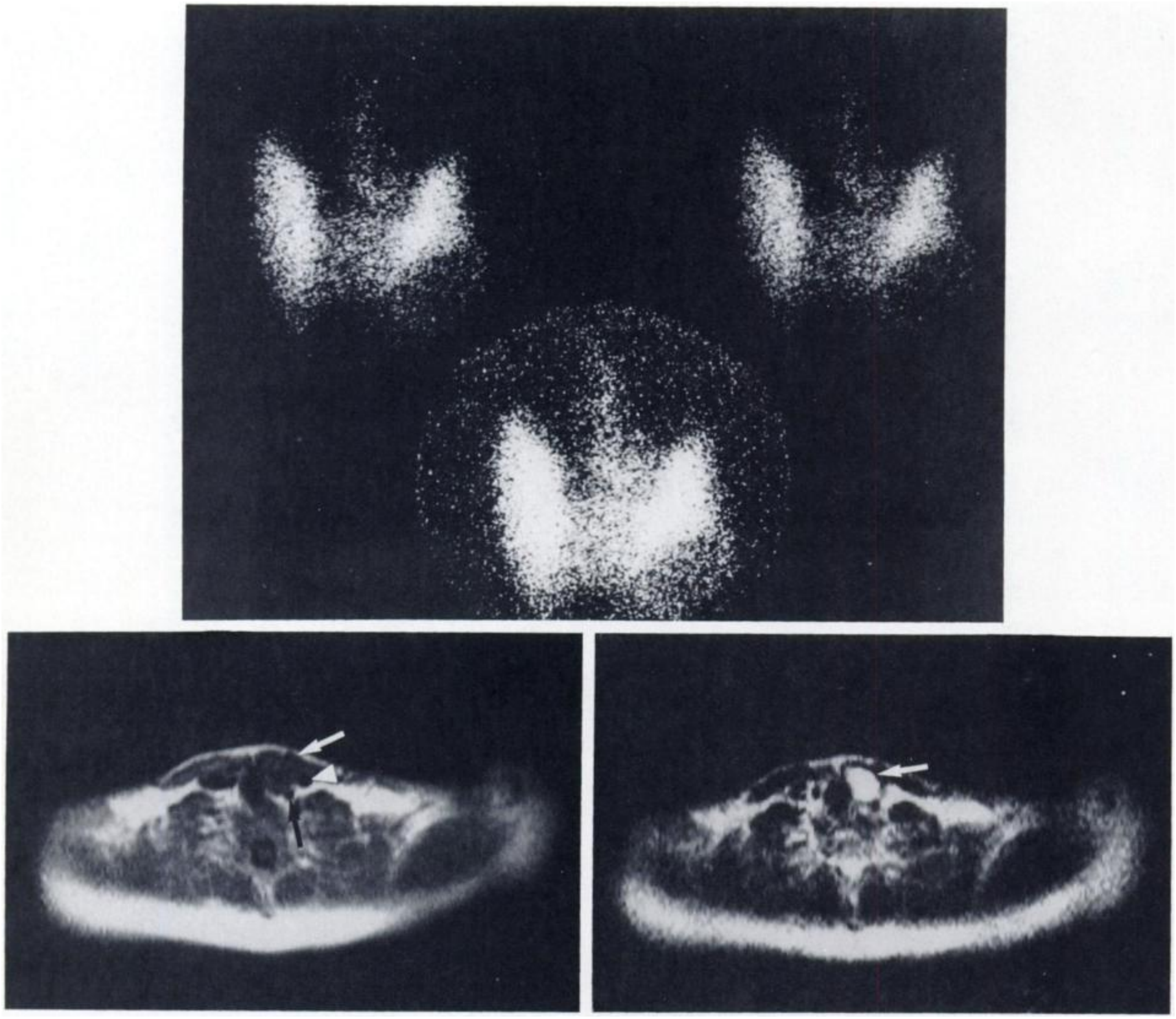

FIGURE 4
Top: Anterior image of [^{99m}Tc]pertechnetate thyroid scan shows area of decreased radionuclide concentration in lower pole of left lobe in patient with hemorrhagic adenoma. Lower left: Transverse MRI image of neck with IR 30/450/1,500 sequence. Left lobe of thyroid is enlarged (white arrow). Internal carotid (black arrow) and internal jugular vein (arrowhead) are well identified. Lower right: MRI image performed at same level with SE 120/1,000 shows increased signal intensity within lower pole of left lobe (arrow). This suggests prolonged T_2 relaxation value of this hemorrhagic adenoma

distinguish blood vessels from lymph node enlargement.

Mediastinum

Respiratory gating, in our experience, has improved image quality in some patients, although cardiac gated MR images in the chest are more easily reproduced and adequate in almost all the patients studied with mediastinal masses. The MR image using SE 30/500 sequence demonstrates the area of abnormal signal intensity on the right side of the mediastinum in a patient with mediastinal lymphoma (Fig. 5A). The right atrium and the left atrium, as well as the descending aorta, can be separated from the rest of the mediastinal structures because of the decreased signal intensity within these structures, secondary to blood flow. In a series of patients studied to evaluate mediastinal and hilar masses, MRI detected additional disease in 25% of the cases when compared with CT (*18*). Magnetic resonance, however, cannot discriminate between neoplastic and inflammatory lymph node pathology by T_1 and T_2 relaxation times, but provides information regarding abnormal lymph nodes analogous to gallium-67 (^{67}Ga) citrate scans (Fig. 5B).

Cardiac imaging using electrocardiographic "R" wave gating has provided excellent image quality (*19*). Since there is no appreciable signal from flowing blood in cardiac chambers, there is a high contrast difference between the myocardial wall and the cardiac chambers.

Congenital cardiac defects are very well defined with high resolution MRI (*20*). A ventricular septal defect is demonstrated in Fig. 6 in the sagittal plane using SE

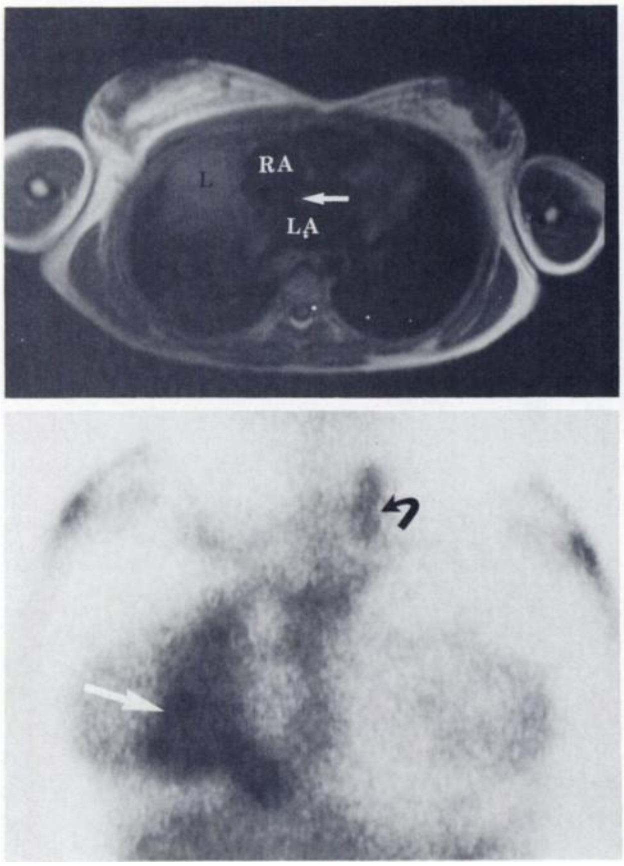

FIGURE 5
Top: Cardiac gated transverse MRI image using SE 30/500 sequence demonstrated abnormally increased signal in mediastinal lymphadenopathy (L) in patient with Hodgkin's disease. Right atrium (RA), left atrium (LA) and atrial septum (arrow) are also shown. Bottom: Anterior view of a [^{67}Ga]citrate scan shows abnormal uptake (arrow) in right side of mediastinum in this patient with Hodgkin's disease. Increased uptake is also seen in the left side of neck (curved arrow)

30/500 cardiac gated image. The cardiac gate can also be used with multislice imaging in transverse, sagittal, or coronal planes. The electrocardiographic R-wave initiates both sequences in the first slice that are followed by multiple slices at fixed intervals which are somewhat similar to multiple frames acquired in a gated radionuclide blood-pool study. The multiple slices thus collected are not only at different levels in the heart, but are also in a different phase in the cardiac cycle.

The potential also exists for MRI to acquire images in cine format to assess focal and global cardiac function. Two-dimensional echocardiography can also provide global functional assessment of the heart with morphological details of the cardiac chamber. Echocardiography is somewhat limited in evaluation of pulmonary venous structures, and in some patients it is technically difficult because of lack of a sonographic window. Pericardial effusions can be detected by MRI (Fig.

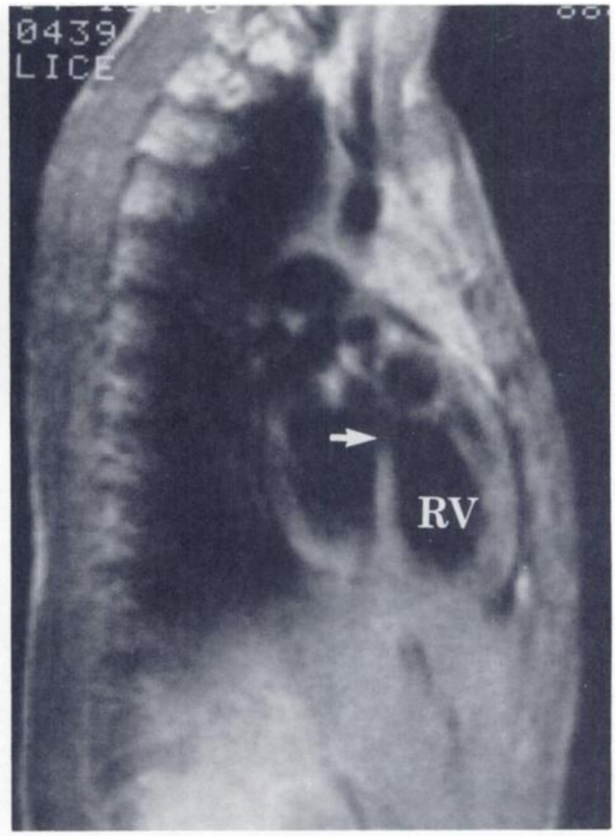

FIGURE 6
Sagittal cardiac gated MRI image demonstrates a ventricular septal defect (arrow) as well as hypertrophied right ventricle (RV) in patient with tetralogy of Fallot.

7A), and further characterized because blood and other proteins in the effusions can affect T_1 and T_2 relaxation parameters. Radionuclide blood pool images (Fig. 7B) can demonstrate pericardial effusion but are not very sensitive and characterization of the effusion is not possible. Initial animal experiments have shown abnormal T_2 relaxation times in myocardial infarction. The infarct can be defined on MR images using intravenous administration of paramagnetic contrast agents (*21*).

Abdomen

Magnetic resonance of the abdomen provides complimentary images to nuclear medicine and has similar transverse imaging capability to CT. Abnormalities in the region of the porta hepatis can be better evaluated with MRI since portal vascular structures are easily identified (*22*). A 33-mo-old child with liver abscess was studied with MRI and an SE 30/500 image demonstrates decrease in signal intensity posteriorly in the right lobe of the liver, suggesting a lesion with increased T_1 relaxation time (Fig. 8A). When MRI imaging was performed at the same level using a T_2 weighted image (SE 62/1,000) the abnormality was identified as an area of increased signal intensity (Fig. 8B). The abnormality seen on the T_2 weighted image involved a larger

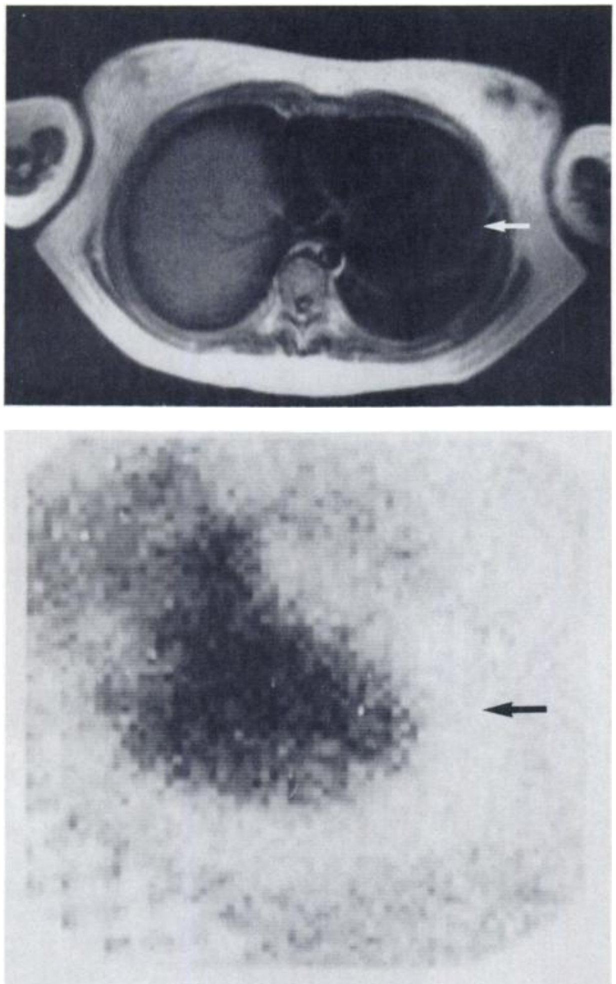

FIGURE 7
Top: Cardiac gated MR image using SE 30/500 sequence demonstrates pericardial effusion (arrow) around heart. Marked decreased signal from effusion suggests fluid with prolonged T_1 relaxation time. Lower: Photopenic area (arrow) around cardiac blood pool in this anterior image is due to large pericardial effusion on ^{99m}Tc-labeled red cell study

area of the right lobe. The increased signal intensity seen with these sequences suggested a longer T_2 relaxation time in the abscess and surrounding edema. Gallium-67 citrate imaging (Fig. 8C) is also a sensitive modality in inflammatory processes but lacks specificity, and the diagnosis is usually made with the use of other associated imaging modalities. Primary and metastatic neoplasms can be detected with MRI although optimal pulse sequences in diagnosing intrahepatic metastases are yet to be determined. The T_1 weighted images, as well as heavily T_2 weighted images, have improved soft-tissue contrast between pathological and normal liver tissue when compared to CT. In addition, the vascular structures within the liver are identified without use of an intravenous contrast agent. Dilated biliary ducts are also differentiated from the vascular structure on T_2 weighted images, since its prolonged T_2 relaxation times demonstrate increased signal intensity on these images, which is contrasted well with markedly diminished signal from the vascular channels (Fig. 9).

Magnetic resonance imaging is useful in patients with diffuse liver disease. Abnormally short T_1 values within the liver in patients with primary biliary cirrhosis may be related to high copper levels (*22*). Extensive iron deposits in the liver result in decreased T_1 and T_2 relaxation times due to the paramagnetic effect of the ferric ion. Similarly, excessive levels of copper within the liver will also decrease the T_1 relaxation time (*23*). This could prove valuable in diagnosing patients with Wilson's disease. Cirrhosis of the liver has also been shown to have prolonged T_1 relaxation time (*24*).

Renal morphology is well evaluated by MRI since the intense signal from fat in the perinephric space provides good contrast. Renal mass lesions can be studied by MRI in coronal, sagittal, and transverse planes. Simple cysts can be diagnosed because of their small borders and prolonged T_1 and T_2 relaxation values (*25*). Magnetic resonance is also used for the examination of

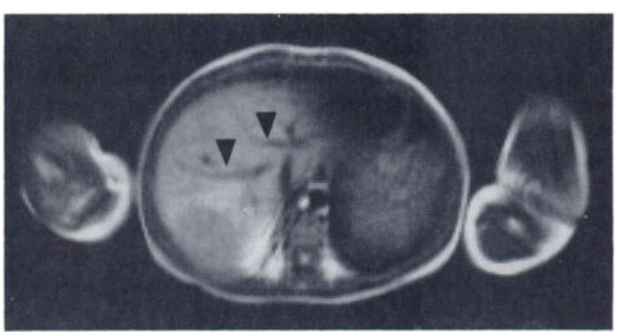

FIGURE 8A
Transverse MR image in child with liver abscess. SE 30/500 sequence reveals area of decreased signal intensity posteriorly in right lobe. Normal vascular structures (arrowheads) are seen in rest of the liver

FIGURE 8B
T_2 weighted image performed in same area using SE 60/1,000 sequence demonstrates marked increased signal in right lobe of the liver. Contrast between abnormality and normal liver is significantly more on T_2 weighted image

primary as well as metastatic tumor in the kidney. Perinephric extension of the primary tumor in perinephric space can be identified with MRI (*25*). Metastatic spread from the renal tumor to the lymph node, the renal vein, and inferior vena cava, as well as bony metastases, can be detected by MRI similar to that of CT. However, unlike CT, no i.v. contrast administration is required with MRI.

Magnetic resonance imaging in a large Wilms' tumor arising from the upper pole of the right kidney is demonstrated in Fig. 10A on SE 30/500 sequence. The coronal image using the same pulse sequence demonstrated displacement of the inferior vena cava towards the left although there was no abnormal signal within

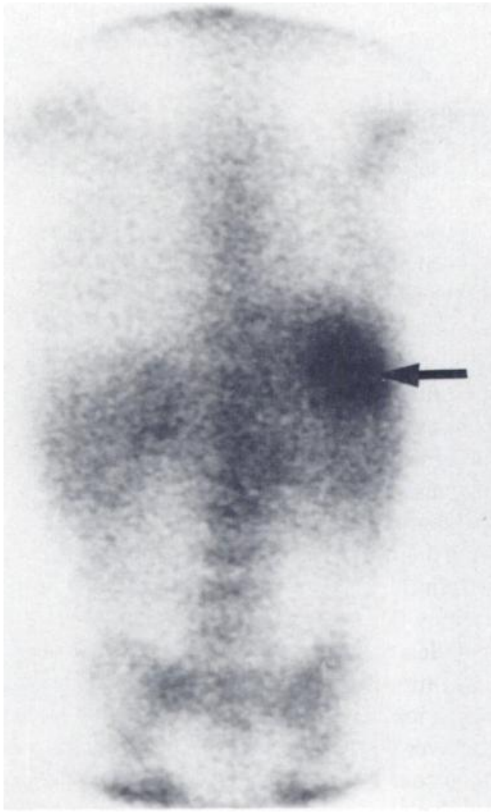

FIGURE 8C
Focal area in right lobe of liver in posterior view has increased activity (arrow) on [^{67}Ga]citrate scan. Abscess has increased activity compared to normal liver uptake of [^{67}Ga]citrate

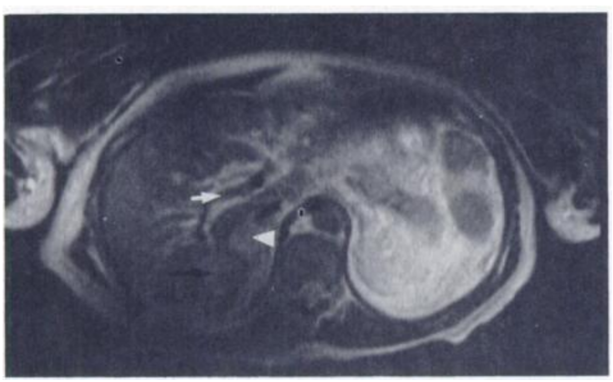

FIGURE 9
Transverse T_2 weighted image (SE 90/1,000) of liver demonstrates excellent contrast between dilated biliary ducts (intense signal = prolonged T_2 relaxation times) and portal vein (white arrow) which does not have appreciable signal due to rapid blood flow. Also demonstrated are metastatic lesion in the liver (black arrow) and adrenal metastasis (arrowhead), both of which have prolonged T_2 relaxation times when compared to normal liver

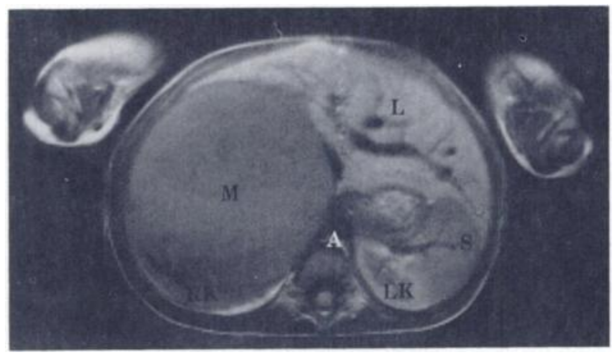

FIGURE 10A
Transverse MR image using SE 30/500 sequence shows a large mass in the right side of abdomen (M) displacing the liver (L) towards left. Portal vasculature is nicely demonstrated. Spleen (S) and top of left kidney (LK) are also shown. Right kidney is distorted (RK) and compressed posteriorly. A = aorta

FIGURE 10B
Coronal SE/500 image reveals large Wilms' tumors displacing and compressing the inferior vena cava (I). There is no evidence of invasion of vena cava by tumor

the inferior vena cava to suggest thrombus or tumor extension within the vessel (Fig. 10B). On the T_2 weighted image (Fig. 10C), the mass had increased in density when compared to the level in the normal portion of the right kidney, and an intense signal within the center of the mass suggested tumor necrosis. Although the NM study (Fig. 10D) could demonstrate abnormalities in the kidney and metastatic spread to the bones, the MRI was extremely useful to evaluate spread of the tumor to perinephric space, liver, lymph nodes and vascular invasion. Abnormal corticomedullary signal is noted on MRI in animal models with surgically-induced renal artery stenosis using T_2 weighted images. Magnetic resonance imaging contrast agents are expected to play a part in the diagnosis of renal artery stenosis. Intravenous administration of either gadolinium diethylenetriaminepentaacetic acid or chromium ethylenediaminetetraacetic acid in animals with surgically-induced renal obstruction have shown distinct differences in the pattern of signal intensity between the normal and abnormal kidney (*21*).

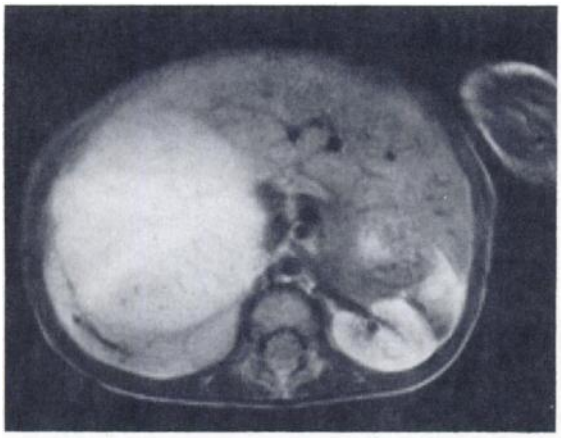

FIGURE 10C
T_2 weighted image demonstrates increased signal intensity from mass compared to liver as well as compressed right kidney. Tumor has increased T_2 relaxation times. Center of mass has intense signal as compared to periphery which is thought to be due to central tumor necrosis

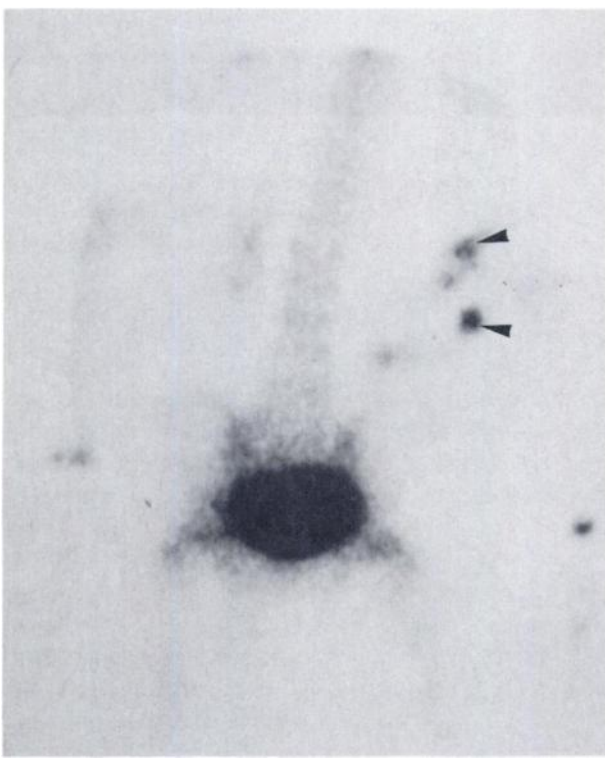

FIGURE 10D
[^{99m}Tc]HDP (hydroxymethylene diphosphonate) bone scan demonstrates no evidence of skeletal metastasis in the posterior view. Marked distortion of renal collecting system (arrowheads) is due large Wilms' tumor

The retroperitoneum and the vascular structures of that area are well visualized using MRI. Lymph node involvement in the retroperitoneum necessary for staging of malignant diseases can also be evaluated by MRI. Patients with an abnormality in the retroperitoneum shown by using [^{67}Ga]citrate scanning can be studied with MRI to demonstrate individual groups of lymph node enlargement. Lymphoma involving the pancreatic group of lymph nodes extending into the liver has also been demonstrated (*26*). Patency of the retroperitoneal vessels can be evaluated with MRI, since normal flow within the vessel does not provide an appreciable signal. Retroperitoneal vessels are identified because they demonstrate excellent contrast with surrounding retroperitoneal fat. Aneurysm, thrombosis, and tumor extension in the vessels are identified. Sagittal and coronal images help to determine tumor

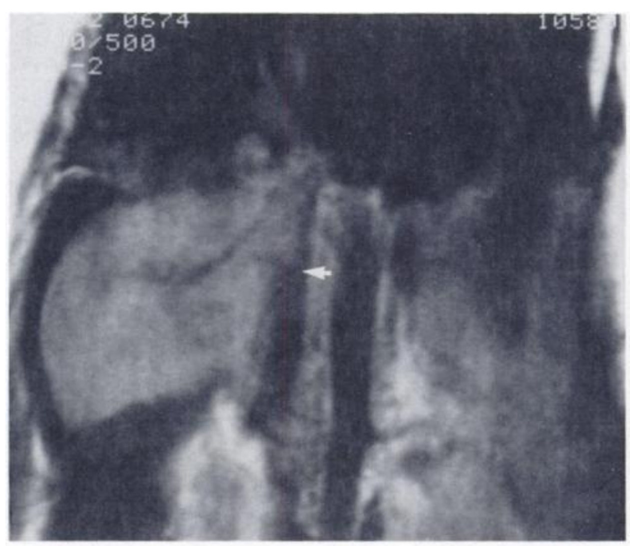

FIGURE 11
Coronal SE 30/500 image shows descending aorta and inferior vena cava similar to anterior projection of arteriogram. Tumor extension of hepatocellular carcinoma into the IVC is identified (arrow)

extension into a vascular structure without use of intravenous contrast agents (Fig. 11).

Skeletal

Although cortical bone is recorded on MR images as an area of markedly decreased signal, the bone marrow produces an intense signal. The skeletal system can also be studied in transverse sagittal and coronal planes. Avascular necrosis of the femur can be diagnosed at an earlier stage on MRI than on conventional radiographs. A patient with avascular necrosis revealed irregularity of the right femoral head in its superior aspect on a coronal SE 30/500 image (Fig. 12A). Cortical bone demonstrated markedly decreased signal but intense signal from the marrow reveals a normal left femoral head (Fig. 12A). The radionuclide bone scan (Fig. 12B) demonstrated increased activity in the right femoral head and a radiograph of the hips was normal. Our initial experience indicates that the radionuclide bone scan may be more sensitive than MRI in the diagnosis of avascular necrosis. A patient with long term steroid therapy showed areas of decreased radioisotope accumulation in both hips and knees (Fig. 13 A and B). Magnetic resonance images of the hips and knees were normal (Fig. 13 C and D). The venous pressure measurements of the hips at the time of surgery were high, confirming the diagnosis of avascular necrosis. Similarly, c'iagnosis of metastases, trauma, and osteomyelitis are superior with MRI when compared to conventional imaging techniques. Magnetic resonance imaging not only provides increased sensitivity, but also demonstrates soft tissue extension of the disease better than conventional radiography. The ability to perform sagittal imaging has shown improved sensitivity to detect bony metastases as compared to routine CT scan, in our experience.

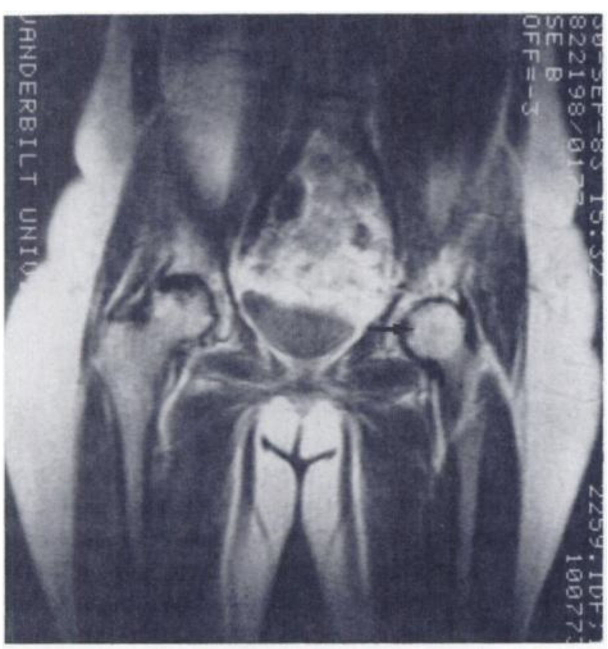

FIGURE 12A
Coronal MRI using SE 30/500 sequence shows marked irregularity of right femoral head in its superior aspect in this patient with avascular necrosis. Left femoral head is normal and has a normal depression medially (arrow) for insertion of ligamentum teres

Although MRI has shown increased sensitivity in detecting skeletal pathology, its ability to differentiate neoplastic lesions from inflammatory or traumatic lesions is yet to be confirmed. In pediatric patients, MRI has demonstrated earlier detection of osteomyelitis than is currently possible radiographically (*27*). Nuclear medicine has shown an increased sensitivity to detecting osteomyelitis when compared to conventional radiographic procedures (*28*). The exact role of these two modalities in the diagnosis of osteomyelitis needs further study. Both benign and malignant primary osseous tumors as well as metastatic disease and inflammatory lesions have shown prolonged T_1 and T_2 relaxation times. In vivo measurements of T_1 relaxation time in pathological lesions have not been able to differentiate inflammatory lesions from neoplastic lesions at present.

In a patient with fracture of the lower tibia which had been undetected for two weeks, the bone scan (Fig. 14A) showed an area of increased activity in the left distal tibia. The MRI demonstrated increased signal intensity on the SE 30/500 image (Fig. 14B), suggesting a prolonged T_1 relaxation time in the lesion. The T_1 weighted image demonstrated a similar area of decreased signal intensity on the ISE sequence (Fig. 14, lower right). An area of abnormality also had increased

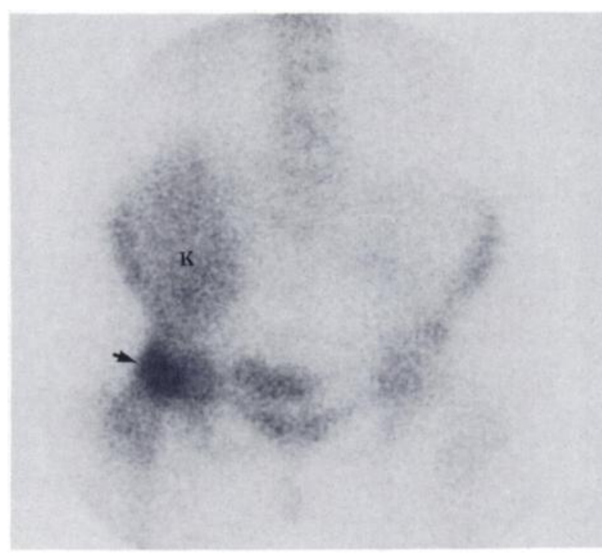

FIGURE 12B
Increased activity in right femoral head (arrow) is seen in anterior view of [^{99m}Tc]HDP bone scan. Radioactivity is also noted in transplanted kidney (K)

T_2 relaxation values when compared to the rest of the bone marrow on SE 120/2,000 image (Fig. 14, lower left). Although osteomyelitis was suspected, there was no evidence of infection at the time of surgery and the cultures grown from the material aspirated from the tibia did not reveal any organisms. Findings on the bone scan and MRI were, therefore, probably due to trauma.

Our early experience regarding use of nuclear medicine and magnetic resonance imaging is summarized in Table 1 in an organ-oriented analysis of these studies

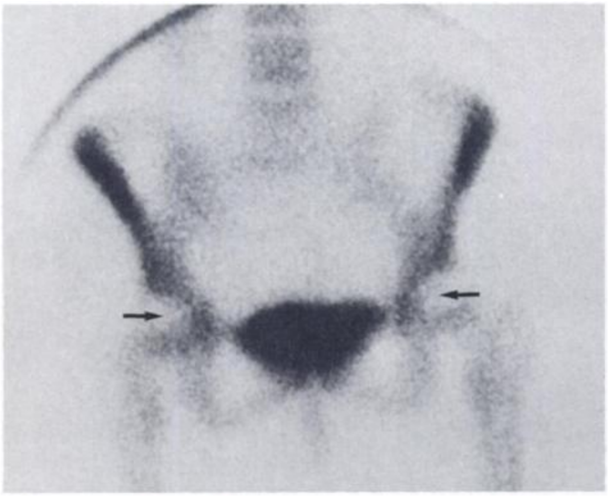

FIGURE 13A
[^{99m}Tc]HDP bone scan in patient with bilateral hip and knee pain and history of systemic lupus erythmatosis. Anterior image of pelvis reveals decreased radioisotope concentration in both femoral heads superiorly (arrows)

FIGURE 13B
Bone scan of knees shows decreased activity in femoral and tibial condyle in right as well as in left knee

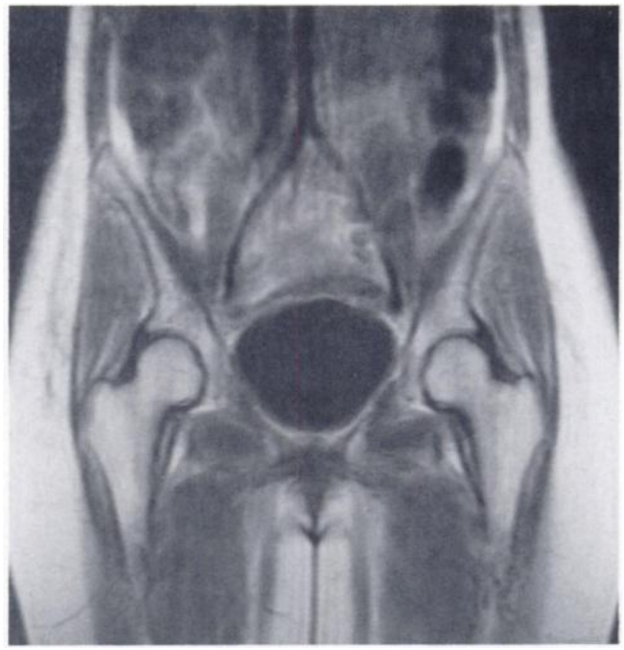

FIGURE 13C
Coronal SE 30/500 sequence in hips shows normal contour of femoral heads, bilaterally

FIGURE 13D
Coronal IR 30/450/1,500 sequence image of both knees also reveal normal surfaces of tibial and femoral condyle. Diagnosis of avascular necrosis was confined by venous pressure measurement at time of surgery

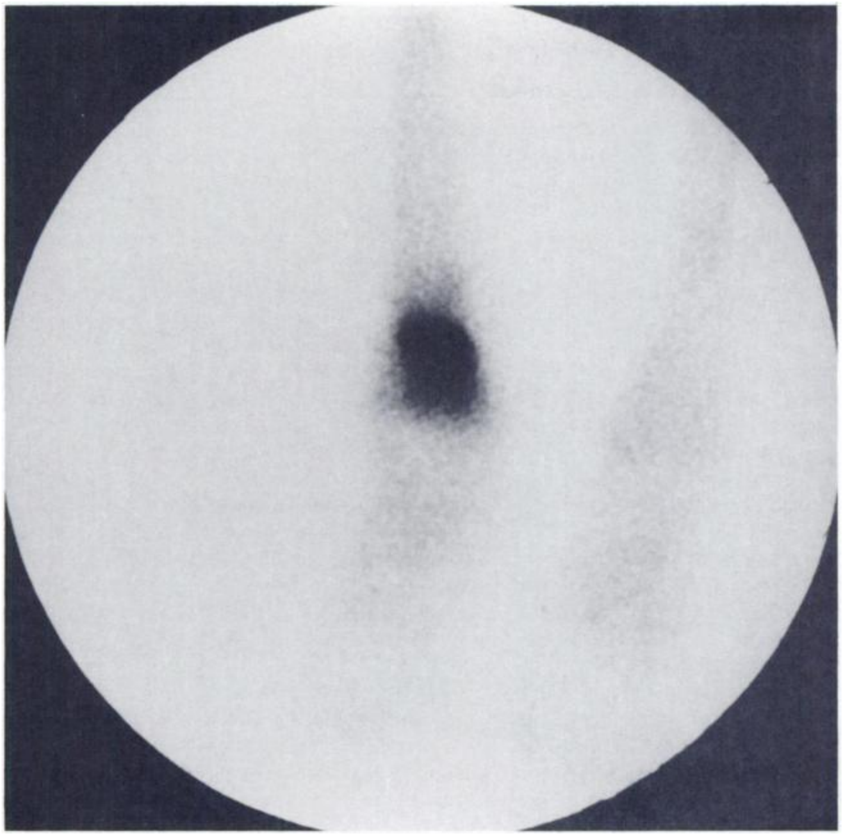

FIGURE 14A
Radionuclide bone scan demonstrates increased activity in lower end of right tibia. [^{99m}Tc]HDP bone scan was performed 2 wk after trauma

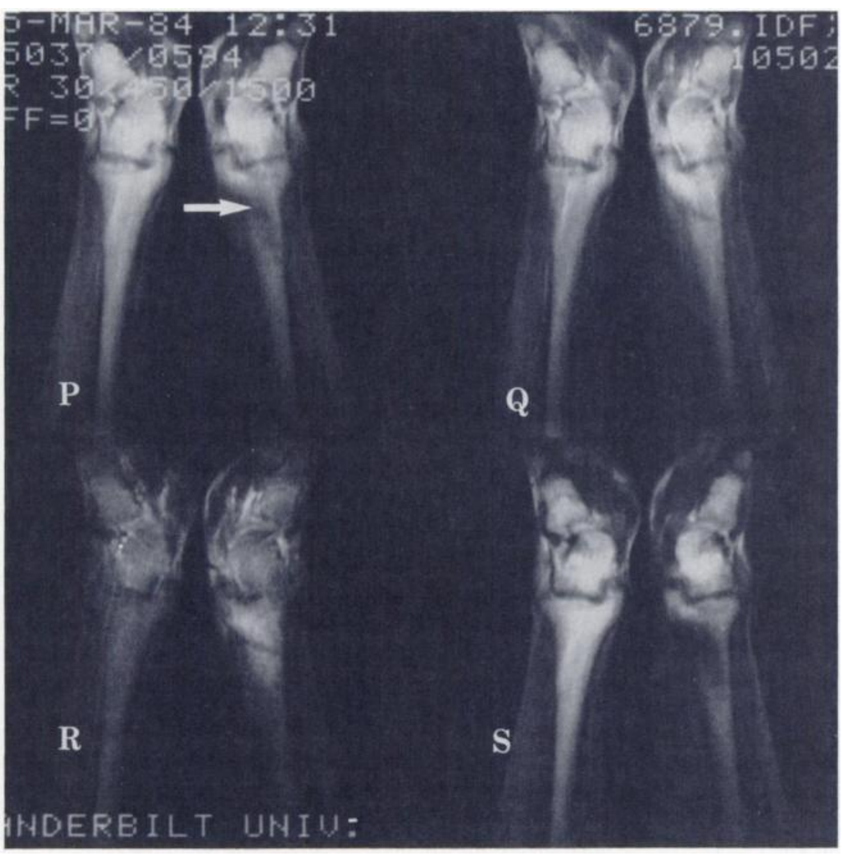

FIGURE 14B
MRI images using different pulse sequences show area of decreased signal intensity (arrow) in distal right tibia on SE 30/500 sequence (P). With increasing T_2 weighting of the image, this area has increased signal intensity when compared to left tibia (Q & R). On T_1 weighted images (S), this area shows decreased signal intensity which represents prolonged T_1 relaxation time

TABLE 1
Summary of Organ-Oriented Analysis of NM and MRI Studies

Organ	Number	Nuclear medicine	Magnetic resonance
Thyroid	7	Classifies nodules on the basis of function and identifies functional substernal thyroid tissue.	Excellent anatomical resolution in multiple planes without evaluation of thyroid function. Substernal extension of functioning thyroid as well as non-functioning thyroid tissue in multiple planes.
Brain	4	Poor anatomic resolution, tumor detection on the basis of interruption of the blood-brain barrier. Early detection of inflammatory lesions such as herpes encephalitis.	Excellent anatomic resolution in multiple planes. Particularly good in posterior fossa and brain stem. Early detection of neoplastic disease and inflammatory disease in the animal model using intravenous contrast agents.
Heart	9	Superior assessment of physiological parameters including ejection fraction, cardiac shunts, ischemic heart disease and regurgitant fraction. Poor anatomical detail.	Superior anatomic resolution due to inherent contrast between blood flow and cardiac walls. Multiplane imaging useful in evaluation of congenital and acquired cardiac defects.
Chest	5	Useful in staging Hodgkins disease although lacks sensitivity in detection of lymphadenopathy.	Excellent anatomic resolution of lymphadenopathy and numerous other mediastinal masses using cardiac or respiratory gating.
Liver	14	Useful in detecting focal as well as diffuse metastatic lesions. Abnormalities in the region of the porta hepatis or vascular invasion very difficult to identify.	Metastatic disease or primary tumors detected using various pulse sequences. Lesions in the region of the porta hepatis and intravascular invasion of the tumor detected without the use of contrast agents.
Kidney	4	Mass lesions are detected although specificity is very poor. Dynamic studies provide physiological parameters for assessment of renal function.	High resolution helps identification and characterization of mass lesions. Vessel invasion is well identified. Assessment of physiological function is poor at the present stage.
Retro-peritoneal	3	Detection of retroperitoneal lymphomatous and inflammatory disease. Abscesses may be detected before anatomical abnormalities have developed.	Diagnosis of retroperitoneal lymphadenopathy and abscesses made without the use of intravenous contrast. Superior spatial resolution. Pancreas is well identified with the use of ferrous gluconate as an oral contrast agent.
Skeletal	10	Radionuclide skeletal imaging very sensitive in detection of tumor, osteomyelitis and avascular necrosis. Lacks specificity.	Multiplane imaging and varying pulse sequences provide early detection of tumor, osteomyelitis and avascular necrosis. Lacks specificity.

and lists the comparative advantages and disadvantages of both modalities.

CONCLUSION

In summary, MRI is a very useful technique in evaluation of intracranial, cervical, thoracic, abdominal, and skeletal pathology. The spatial resolution of MRI is similar to CT and ultrasound, but the improved soft tissue contrast increases lesion detectability. Although tissue characterization of MRI on the basis of T_1 and T_2 relaxation parameters alone is in the early stages of development, the use of in vivo spectroscopy will improve MRI diagnostic capabilities. The ability to perform imaging with carbon-13, phosphorus-31, and sodium-23 will generate additional biochemical and physiological information (*31*). Oral and organ targeted contrast agents will further aid in both static and dynamic images (*29*). The use of surface coils will improve both spatial resolution and lesion detectability in small organs such as the thyroid and parathyroid glands. Evaluation of blood flow by MRI using different pulse sequences, as well as gated cardiac images in cine format, will add to functional information, similar to that obtained by nuclear medicine examinations. The role of MRI as a primary investigational modality and its complementary role with nuclear medicine and other imaging modalities requires further evaluation with larger series of cases for individual disease processes. Comprehensive discussion of the current role and future clinical potential for MRI appears in a recent text on this subject (*32*).

ACKNOWLEDGMENTS

The authors acknowledge technologists Jill Craig and Oscar Wolfe for assisting with the clinical examinations, Val Runge, MD and W. Hoyt Stephens, MS for technical insights, Bonnie Norman, Carolyn Cooper, Margaret Moore, Joann Fields and May Person for assisting with manuscript preparation, and Mary Henry for final editing.

REFERENCES

1. Margulis AR, Higgins CB, Kaufman L, et al: *Clinical Magnetic Resonance Imaging*. San Francisco Radiology Research Education Foundation, 1983

2. Kressel HY, Axel L, Glover G, et al: Coronal nuclear magnetic resonance (NMR) imaging of the abdomen at 0.5 tesla. *J Comput Assist Tomogr* 8(1):29-31, 1984
3. Damadian R: Tumor detection by NMR. *Science* 171:1151, 1971
4. New PF, Rosen BR, Brady TJ, et al: Potential hazards and artifacts of ferromagnetic and nonferromagnetic surgical and dental materials and devices in nuclear magnetic resonance imaging. *Radiology* 147:139-148, 1983
5. Pavlicek W, Geisinger M, Castle L, et al: The effects of nuclear magnetic resonance on patients with cardiac pacemakers. *Radiology* 147:149-153, 1983
6. Patton JA, Lagan JE, Price RR, et al: NMR site planning and patient safety. In *Nuclear Magnetic Resonance and Correlative Imaging Modalities,* Partain CL, ed. New York, Society of Nuclear Medicine, Inc., 1984
7. Jones JP, Partain CL, Mitchell MR, et al: *Principles of Magnetic Resonance.* In *Magnetic Resonance Annual,* Kressel HY, ed. New York, Raven Press, 1985
8. Koutcher JA, Burt CT: Principles of nuclear magnetic resonance. *J Nucl Med* 25:101-111, 1984
9. James AE, Partain CL, Holland GN, et al: Nuclear magnetic resonance imaging: The current state. *Am J Roentgenol* 138:201-210, 1981
10. Partain CL, Price RR, Patton JA, et al: Overview of nuclear magnetic resonance imaging: Physical principles, clinical potential, and interrelationship with radionuclide imaging and other modalities. In *Nuclear Magnetic Resonance and Correlative Imaging Modalities,* Partain CL, ed. New York, Society of Nuclear Medicine, Inc., 1984
11. Bydder GM, Steiner RE, Young IR, et al: Clinical NMR imaging of the brain: 140 cases. *Am J Roentgenol* 139:215-236, 1982
12. Runge VM, Price AC, Kirshner HS, et al: The evaluation of multiple sclerosis by magnetic resonance imaging. *Am J Roentgenol* 143:1015-1025, 1984
13. Mills CM, Crooks LE, Kaufman L, et al: Cerebral abnormalities. Use of calculated T_1 and T_2 magnetic resonance images for diagnosis. *Radiology* 150:87-94, 1984
14. Araki T, Inouye T, Suzuki H, et al: Magnetic resonance imaging of brain tumors: Measurement of T_1. *Radiology* 150:95-98, 1984
15. Stark DD, Moss AA, Gamsu G, et al: Magnetic resonance imaging of the neck. Part II: Pathologic findings. *Radiology* 150:455-461, 1984
16. Bushist B, Ellis K, Gold RP: Computed tomography of intrathoracic goiter. *Am J Roentgenol* 140:455-460, 1983
17. Sandler MP, Patton JA, Sacks GA, et al: Evaluation of intrathoracic goiter with I-123 scintigraphy and nuclear magnetic resonance imaging. *J Nucl Med* 20:874-876, 1984
18. Cohen AM, Creviston S, LiPuma JP, et al: NMR evaluation of bilar and mediastinal lymphadenopathy. *Radiology* 148:739-742, 1983
19. Lanzer P, Botvinick EH, Schiller NB, et al: Cardiac imaging using gated magnetic resonance. *Radiology* 150:121-127, 1984
20. Fletcher BD, Jacobstein MD, Nelson AD, et al: Gated magnetic resonance imaging of congenital cardiac malformation. *Radiology* 150:137-140, 1984
21. Runge VM, Clanton JA, Price AC, et al: Paramagnetic contrast agent in magnetic resonance imaging. Research and clinical experience at Vanderbilt University. *Physiol Chem Phys Med NRM:* in press
22. Doyle FH, Pennock JM, Banis LM, et al: Nuclear magnetic resonance imaging of the liver: Initial experience. *Am J Roentgenol* 138:193-200, 1982
23. Runge VM, Clanton JA, Smith FW, et al: Nuclear magnetic resonance of iron and copper disease states. *Am J Roentgenol* 141:943-948, 1983
24. Buonocore E, Borowski GP, Pavlicek W, et al: NMR imaging of the abdomen. Technical considerations. *Am J Roentgenol* 141:1171-1178, 1983
25. Kulkarni MV, Shaff MI, Sandler MP, et al: Evaluation of renal masses by MR imaging. *J Comput Assist Tomogr* 8(5):861-865, 1984
26. Kulkarni MV, Partain CL, Tishler JM, et al: Magnetic resonance imaging of the abdomen. In *NMR Imaging: An Introduction.* Rinck P, ed. Stuttgart, Georg Thieme: in press
27. Fletcher BD, Scoles PV, Nelson AD: Osteomyelitis in children: Detection by magnetic resonance. *Radiology* 150:57-60, 1984
28. Gilday DL, Paul DJ, Paterson J: Diagnosis of osteomyelitis in children by combined blood pool and bone imaging. *Radiology* 117:331-335, 1975
29. Runge VM, Clanton JA, Price AC, et al: Contrast enhanced magnetic resonance evaluation of a brain abscess model and comparison with computed tomography. *Am J Roentgenol*: in press
30. Patton JA, Sandler MP, Partain CL: Prediction of benignancy of the solitary "cold" thyroid nodule by fluorescent scanning. *J Nucl Med* 26:461-464, 1985
31. Burt CT, Koutcher JA: Multinuclear NMR studies of naturally occurring nuclei. *J Nucl Med* 25:237-248, 1984
32. Partain CL, James AE, Rollo FD, et al: *Nuclear Magnetic Resonance (NMR) Imaging.* Philadelphia, W. B. Saunders Co., 1983